Check for updates

# Local time-dependent microstructure of aging TEMPO nanofibrillated cellulose gel
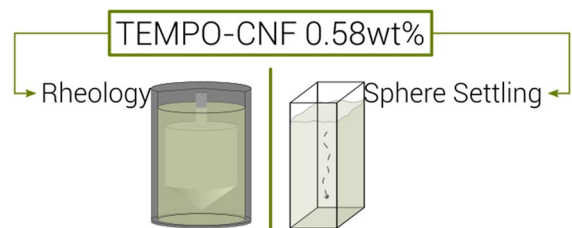
**Hakimeh Koochi** [ORCID] · **Jonatan Mac Intyre** ·
**Leevi Viitanen** · **Antti Puisto** ·
**Nahid Maleki-Jirsaraei** · **Mikko Alava**

**Abstract** The aging behavior of TEMPO-CNF suspensions is investigated using rheological measurements and experiments involving the free-falling solid sphere. The properties of CNF suspensions, which are formed of water and cellulose fibers with a large aspect ratio, are fundamentally different from those commonly known as model low-density gels. We characterize their aging utilizing SAOS rheometry following a period of shear rejuvenation, measuring the effect of aging time on the observed stress overshoot, and additionally measure the rheological hysteresis under continuous shear. In addition to such tests, which probe the sample at the bulk level, we study their local aging behavior via the Stokes' experiment. During SAOS, the aging of the material results in a logarithmic growth of the elastic modulus over the first 50 minutes. In the Stokes' experiment, depending on the sphere size, we find a systematic decrease in the sphere velocity with aging times up to 16 days and identify a range of intermittent particle motion. Based on our experimental evidence, we propose that the aging effect within the TEMPO-CNFs occurs due to the restructuring of fibrous elements by Brownian diffusion and that the aging of the system does not develop homogeneously across the whole sample as a consequence of the wide size distribution of CNFs. Finally, we note that this may be one of the primary reasons why the rheological data on even the same batch of CNFs show a large scatter.

**Graphical abstract**

H. Koochi (✉) · J. Mac Intyre · L. Viitanen · M. Alava
Department of Applied Physics, Aalto University, School of Science, P.O. Box 11100, 00076 Aalto, Finland
e-mail: hakimeh.koochi@aalto.fi

J. Mac Intyre
e-mail: jonatan.macintyre@aalto.fi

L. Viitanen
e-mail: leevi.viitanen@aalto.fi

M. Alava
e-mail: mikko.alava@aalto.fi

H. Koochi · N. Maleki-Jirsaraei
Department of Physics, Alzahra University, Faculty of Physics and Chemistry, Tehran 1993891167, Iran
e-mail: maleki@alzahra.ac.ir; nahid.maleki@gmail.com

A. Puisto
VTT Technical Research Centre of Finland Ltd, Espoo, Finland
e-mail: antti.puisto@vtt.fi

TEMPO-CNF 0.58wt%
Rheology — Sphere Settling

**Keywords** TEMPO-CNFs · Aging · Thixotropy · Rheology · Sphere settling

## Introduction

Low-density gels exhibiting yield stress and time - dependent elasto-viscous features are ubiquitous in practical applications such as food, biomedicine, and energy industries (Li et al. 2021). Therefore, developing environmentally friendly, sustainable, and renewable alternatives for applications in these fields is crucial. To this end, highly refined cellulose materials, including cellulose nanofibers (CNFs), cellulose microfibers (CMFs), TEMPO-oxidized cellulose nanofibers (TEMPO-CNFs), and cellulose nanocrystals (CNCs), could be utilized further. From a rheological perspective, these materials possess fascinating properties. In general, they are shear-thinning, but their accurate characterization is sensitive to concentration, morphology, the size distribution of fibers, temperature, and manufacturing processes (Li et al. 2021; Liao 2021). For instance, CNF suspensions display yielding behavior where the yielding point is a function of shear history and solid content (Poling-Skutvik et al. 2020; Iotti et al. 2011). Similar to the behavior of other low-density suspensions, their shear rheology exhibits hysteresis typically at shear rates below $100 \text{ s}^{-1}$. This hysteresis is specifically characteristic of thixotropic fluids (Divoux et al. 2013; Barnes 1997). At higher temperatures beyond 60 °C, the hysteresis vanishes. This is accompanied by a decrease in viscosity in some CMF samples (Iotti et al. 2011). Such hysteresis is dependent on the solid concentration: no thixotropic or hysteretic behavior has been reported for TEMPO-CNFs at low concentrations (Liao 2021; Iotti et al. 2011; Sanandiya et al. 2019). Moreover, rheological studies of these materials using oscillatory shear have sometimes identified linear viscoelastic regions and gel-like behavior depending on the morphology and concentration of the sample (Nechyporchuk et al. 2016; Lasseuguette et al. 2008; Liao et al. 2021).

CNF suspensions possess a wide particle size distribution ranging from 1 to 50 nm (diameter) and 1 to 100 µm (length), resulting in an aspect ratio from 100 to 2000 (Liao 2021; Hubbe et al. 2017). In contrast, TEMPO-CNFs contain fibers of the size range of $3 - 5 \text{ nm}$ diameter, $0.5 - 10 \text{ µm}$ length, and $300 - 1000$ aspect ratio (Liao et al. 2021; Isogai et al. 2011; Levanic et al. 2020; Nechyporchuk et al. 2014; Šebenik et al. 2019). The diffusion time scales associated with such particle size distribution imply

spatially non - homogeneous thixotropic evolution, particularly when an imperfect mixing of the material occurs (Mohtaschemi et al. 2014).

In TEMPO-CNFs, the combination of such complex rheology becomes further complicated by the fiber's internal structure and water swelling resulting in peculiar flow behavior in shear flow (Liao et al. 2021; Fneich et al. 2019; Pääkkönen et al. 2016; Dimic-Misic et al. 2013). Against this background, we present an experimental analysis specifically on the non-trivial time-dependent rheological behavior of TEMPO-CNFs, which has not been sufficiently examined. Our study aims to yield new information on the aging and rejuvenation processes of TEMPO-CNFs (Šebenik et al. 2019). We approach the problem by rheological characterization and analysis of the dynamics of a free-falling solid object through the aged samples.

Among the well-known low-density gels, Laponite exhibits comparable rheology to TEMPO-CNFs. Therefore, creating a mixture of these two substances may satisfy the required gel property for some biomedical applications (Šebenik et al. 2020). Laponite gels were the subject of several studies involving Stokes' experiment. For the first time in 2004, steel spheres with a diameter of 3 mm were submerged into Laponite RD® suspensions (3 wt%), that had aged for around 40 min. The experiment displayed a continuously decreasing velocity with time and verified that in the presence of thixotropy, the disturbed area surrounding the sphere dominates the settling behavior (Ferroir et al. 2004). Later, characterization based on examining the flow field in Laponite (2.5 wt%) with a range of aging times between $30 - 220 \text{ min}$, conducted the breaking of the flow field fore-aft symmetry dependent on both the aging time and the stress exerted by the solid object (Gueslin et al. 2006). In addition, the observed fluidized layer around the solid object becomes thinner with aging (Tabuteau et al. 2007; Gueslin et al. 2006). Further investigations discovered that viscoelasticity has a significant impact on the fore-aft symmetry breaking that is characterized by a negative wake behind the sphere (Gueslin et al. 2009). This is reminiscent of the viscoelastic overshoot familiar from non-thixotropic complex fluids, such as foams (Arigo and McKinley 1998; Dollet and Graner 2007; Viitanen et al. 2019). Further research in the field has reported an irregular quasi-periodic speed regime for a 3 mm steel sphere

in Laponite B® (1.5 wt%) and it concluded to be the result of shear banding (Fazilati et al. 2017). Furthermore, inserting $2 - 6$ mm spherical steel objects in Laponite XLG® (2.8 wt%), aged for $1 - 3$ h, displayed regimes of either decreasing or increasing velocity. These regimes may or may not reach a steady state where the microstructure breakage rate governs the motion (Biswas et al. 2021).

Generally, the complex shear flow and the associated settling regimes are dependent on the concentration, the Laponite variant, as well as aging and solid-phase characteristics. This behavior is also in stark contrast to a simple yield stress microgel such as Carbopol, that beyond the critical stress, a terminal settling velocity is expected (Tabuteau et al. 2007; Putz et al. 2008; Sgreva et al. 2020). Similar settling behavior as in Laponite was also observed in other non-Newtonian fluids. For instance, in a Xanthan suspension, which is thixotropic, viscoelastic, and shear-thinning, the time dependence of the viscosity was shown to dictate the velocity of the solid sphere (Moseley et al. 2019). Going beyond thixotropic fluids, in a dense cornstarch suspension, a typical rheopectic fluid, the formation, and relaxation of a jammed layer under the object were demonstrated to produce an oscillatory settling velocity ending in a stop-go cycle (Von Kann et al. 2011).

The literature reports cooperative rheological models extended to explain solid-fluid interactions (Ferroir et al. 2004; Fazilati et al. 2017; Biswas et al. 2021; Moseley et al. 2019; Von Kann et al. 2011). However, finding an accurate link between the Stoke's experiment and rheological data has proven to be difficult, since the two experiments typically probe the sample properties at different scales (Gueslin et al. 2009). Besides considering the essential influence of rheology, the local particles configuration and their morphology may significantly alter interactions (Sgreva et al. 2020).

In this study, we first characterize the TEMPO-CNFs following the protocols of rheological measurements proposed in Divoux et al. (2011, 2013). Then, we proceed to the settling experiments where we vary the aging time of the fluid and the size of the sphere. As far as we know, this is the first study of its kind for TEMPO-CNFs. We characterize the yield properties of the fluid by finding the smallest particle able to penetrate the sample. Observation of different irregularities in the motion of the solid sphere shows that

the size distribution of the fibers induces variations in the local rheological properties, which tend to be magnified by the aging time. The experimental observations are reflected based on a modeling approach that involves thixotropy.

The article is organized as follows. First, we explain our material and methodology. Next, the rheological characterization and settling behavior are discussed. Finally, we present our conclusions.

## Materials and methods

### Materials

We used TEMPO-CNFs with a concentration of 1.16 wt% produced from softwood Kraft pulp by VTT (Finland) (Pöhler et al. 2020; Leppiniemi et al. 2017; Skogberg et al. 2017). Since the gel-like suspension was highly dense for our settling experiments, we diluted the suspension with high purity Finnish tap water down to a 0.58 wt% fibril concentration. The density of the final solution was $\rho_f = 1057 \, \text{kg} \cdot \text{m}^{-3}$. To form a homogenized sample, it was gently mixed using a mechanical stirrer at low speed for 3 h. Then, it was deposited in a rectangular glass container and mixed again for an extra 30 min. During the mixing process, small air bubbles were created in the suspension. Therefore, the suspension was left to rest at a low temperature (6 °C) for one week, during which the bubbles would coarsen and rise to the top of the container.

### Rheological measurements

The suspension was characterized by utilizing Antor-Paar MCR302 rheometer with a special serrated bob and cup geometry. A grooved geometry was used to reduce the effects of wall slip (gap width 5.22 mm). Each time, the suspension was mixed for 2 min before filling the cup and then left to rest for one hour at room temperature. A pre-shear of $10^3$ s$^{-1}$ for 300 s was applied before each rheological test to reset the shear history.

We run two different protocols of measurement. The first was a flow curve with the shear rate between $\dot{\gamma}_{min} = 10^{-3}$ s$^{-1}$ to $\dot{\gamma}_{max} = 10^3$ s$^{-1}$ through $N$ successive logarithmically spaced steps of duration $\delta t$ (Divoux et al. 2013). The flow curves are measured first with

decreasing shear rate ramp, then immediately followed by an increasing shear rate ramp. The second measurement was a Small Amplitude Oscillatory Shear (SAOS) test using an oscillatory frequency $f = 1$ Hz and a strain of $\gamma = 0.01$ followed by a shear start-up. Time-dependent SAOS test and stress variation of shear start-up were carried out at several steps $N$ and shear rates $\dot{\gamma}$.

Settling of spheres

Figure 1 shows the experimental setup. The TEMPO-CNF 0.58 wt% was placed in a rectangular glass container of dimensions $0.15 \times 0.15 \times 0.5$ m and a piston plate with several holes of diameter 0.4 mm was
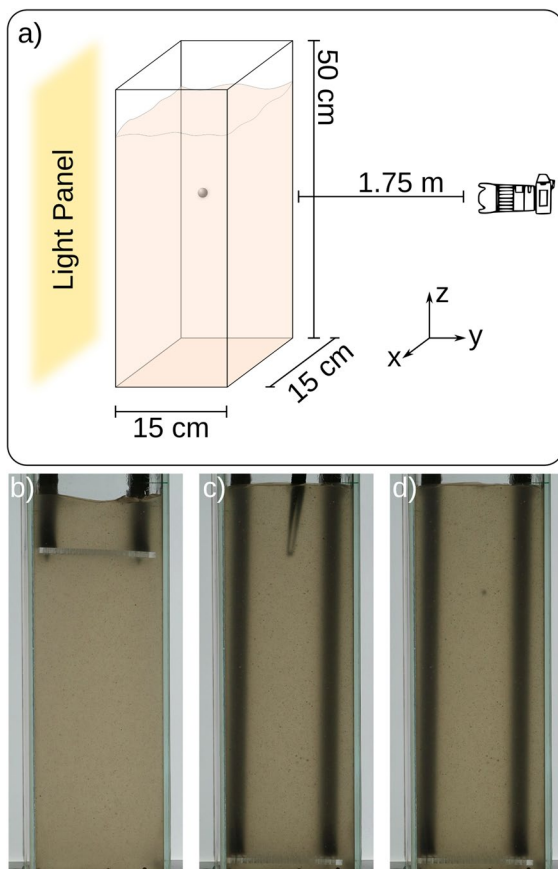


**Fig. 1** **a** Schematic of the experiment setup. The rectangular tank containing the fluid is 50 cm high and 15 cm wide. **b-d** Photograph of the settling process inside the container: The suspension was mixed using a piston (**b**) for 4 min. The solid steel sphere was placed in the initial position (**c**) and left to settling (**d**)

used to mix the suspension before each measurement (Fig. 1b) and reset the shear history. Next, we left the suspension to rest at 6 °C to introduce an aging time $t_a$ (0 s to 16 days). The imaging is implemented using a Canon M3 camera, which takes compressed video at $1920 \times 1080$ pixels using the h.264 encoding. The camera was positioned perpendicular and at a fixed distance of 1.75 m to the container. The videos were analyzed using a custom-made MATLAB script that tracks the object using standard procedures.

For each experiment, one sphere was released without initial velocity and placed at least 0.05 m away from the container's walls to avoid any wall-particle interaction (Fig. 1c). We used solid steel spheres of density equal to $\rho_s = 7800$ kg · m$^{-3}$ and a diameter $d_s$ that ranges between $3.5 - 8$ mm (Fig. 1d). At each stage, care was taken to avoid any evaporation by sealing the container appropriately.

## Rheological characterization

Figure 2a shows the flow curve obtained by first decreasing the shear rate (arrow down) in $N = 90$ logarithmically spaced steps with a duration time of $\delta t = 5, 10, 50, 100$ s per point, and then increasing the shear rate (arrow up). For the smallest duration time, we observed a slight hysteresis between decreasing and increasing shear-rate sweeps for $\dot{\gamma} \leq 1$ s$^{-1}$. Furthermore, the size of the hysteresis cycle increases as the duration time $\delta t$ is increased from 5 to 100 s. In line with other studies across the whole range of cellulose-based suspensions, at low shear rates, the flow curve of up-sweep lies under the down-sweep. According to the present understanding this is related to wall slip (Iotti et al. 2011; Koponen 2020; Saarinen et al. 2014; Nechyporchuk et al. 2014; Martoïa et at. 2015).

The rheology of yield stress fluids is often modeled using the Herschel-Bulkley model:

$$\sigma = \begin{cases} \sigma_T + K\dot{\gamma}^n & \sigma > \sigma_T \\ 0 & \sigma \leq \sigma_T \end{cases} \tag{1}$$

Figure 2b shows that the flow curve, neglecting the aging effects, may be fitted by such a simple model. Here, the fitting parameters are $\sigma_T = 20.65$ Pa, $K = 11.18$ Pa · s$^n$ and $n = 0.358$. While $n$ is constant for different measurement times, $\sigma_T$ and $K$ decrease when $\delta t$ increases. Note that given the thixotropic
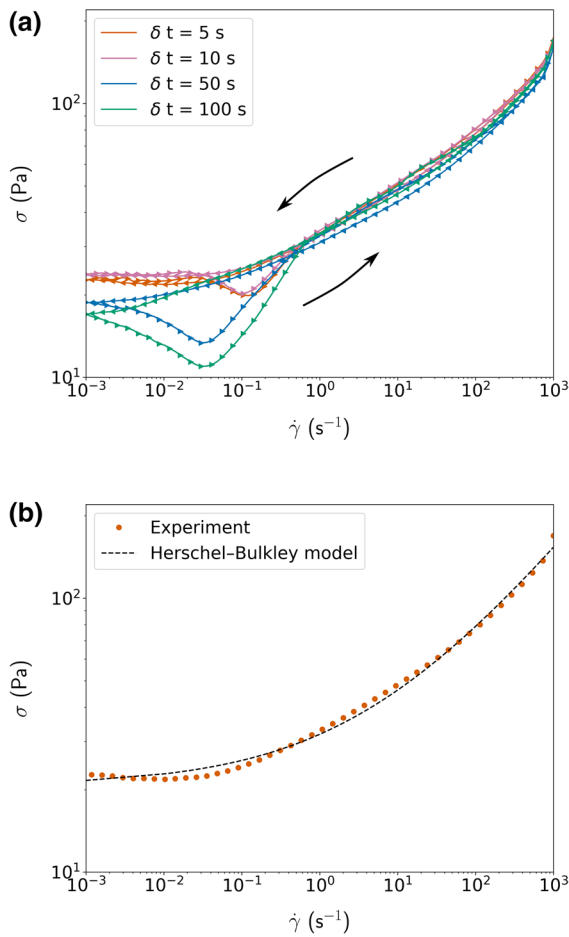
**Fig. 2** **a** Flow curves $\sigma$ versus $\dot{\gamma}$ obtained by first decreasing the shear rate from $10^3$ to $10^{-3}$ s$^{-1}$ in $N = 90$ logarithmically spaced steps of duration $\delta t$ each, and then increasing $\dot{\gamma}$ over the same range. Each curve corresponds to a different time interval per step. **b** The experimental data can be fitted with a Herschel-Bulkley model (dashed black line). The exponent is $n = 0.358$

**Table 1** Fitting parameters for the storage modulus $G'$ shown in Fig. 3a

| $t$ (min) | $G'_0$ (Pa) | $a$ (Pa) |
|---|---|---|
| 5 | 64.27 | 6.54 |
| 15 | 63.57 | 7.04 |
| 20 | 62.24 | 7.13 |
| 50 | 59.82 | 7.75 |



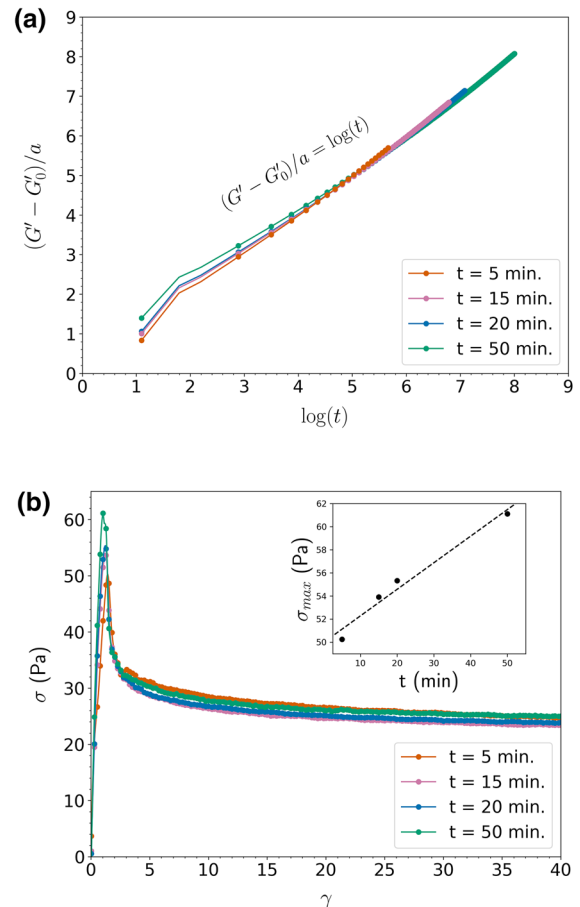**Fig. 3** **a** Storage modulus $G'$ in SAOS test increases logarithmically with the waiting time between initial applied pre-shear of $1000$ s$^{-1}$ (for 300 s) and the following shear start-up test. The oscillation frequency is $f = 1$ Hz, the strain amplitude is $\gamma = 0.01$ and the temperature is $T = 22$ °C. **b** Shear stress $\sigma$ versus shear strain $\gamma$ in the shear start-up test. A shear rate $\dot{\gamma} = 0.25$ s$^{-1}$ was imposed at $t = 0$ s after the SAOS test, Fig. 3a). The overshoot increases with the aging time $t$ (inset)

nature of the suspension, we do not expect that the Herschel-Bulkley model is capable to fit the hysteresis loop (Iotti et al. 2011).

Next, to probe the dynamics of the structure aging and rejuvenation, we carry out a SAOS test followed by a shear start-up, and the results of both tests are shown in Fig. 3. First, we performed the SAOS using an oscillation frequency $f = 1$ Hz and strain amplitude $\gamma = 0.01$ at 22 °C after a pre-shear of $1000$ s$^{-1}$ for 300 s . Here, the structure of the sample is first broken, and then SAOS is used to monitor the structure build-up for different waiting times, $t$. The storage

modulus is considered as an appropriate measure reflecting the state of the structure. Figure 3a shows how the $G'$ increases with time as the sample relax after pre-shearing. We observed that the storage modulus $G'$ grows logarithmically with time as seen in Fig. 3a (the fitting parameters are presented in Table 1).

At the end of the SAOS measurement, we applied a shear start-up where a constant shear rate $\dot{\gamma} = 0.25$ s$^{-1}$ is imposed at $t = 0$ s. The shear stress $\sigma$ is monitored as shown in Fig. 3b. It follows a well-known viscoelastic response: the stress initially increases linearly with time before passing through a maximum and finally decreases to a steady-state value. However, in this case, one must note the small drift in the shear stress even after $\gamma = 35$, which is the manifestation of thixotropy. Another observation is the increase of the stress overshoot with aging time $t$ that is associated with the increase of $G'$ (Fig. 3b inset).

Now, we turn our attention to the shear start-up response of the TEMPO-CNFs under different shear rates. When following the previously introduced protocol of imposing the initial pre-shear of 1000 s$^{-1}$ to reset the microstructure, and then applying a SAOS test at a constant waiting time of $t = 15$ min, this time the storage modulus $G'$ appears approximately the same for all cases. The consequent shear start-up result at different imposed shear rates is shown in Fig. 4. Effectively, both the stress overshoot $\sigma$ (Fig. 4 inset) and its corresponding strain value increase with the shear rate $\dot{\gamma}$. Note the dependence of the stress on shear rate, which roughly aligns with the data in Fig. 2. For a simple yield stress fluid, the maximum stress overshoot occurs at relatively the same values of strain (Benzi et al. 2021). In the TEMPO-CNFs, this is not the case, but the maximum slightly shifts towards higher values of strain, visible even at such a modest shear rate range.

## Sphere settling

We carried out a total of 67 experiments to observe the different behaviors of sphere settling with aging. According to our observations, the motion of the sphere along the $x$- and $y$-axis is negligible. Thus, the analysis focuses along the $z$-axis. Then, we sort the sphere behaviors based on the $\ell_z$ displacement. Examples of the different trajectories are shown
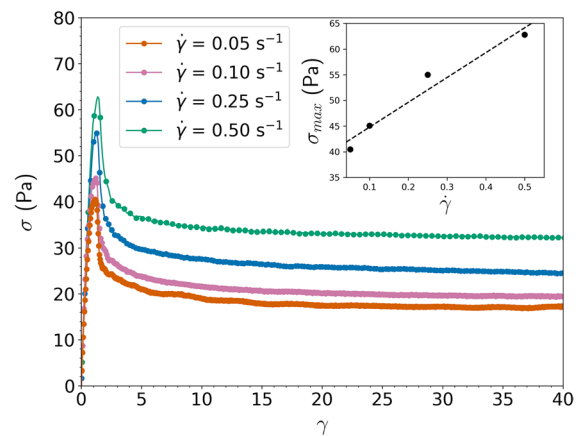


**Fig. 4** Shear stress $\sigma$ versus shear strain $\gamma$ in a shear start-up test. Before the measurement, first a pre-shear of 1000 s$^{-1}$ for 300 s was imposed, and then a SAOS test with an oscillatory frequency $f = 1$ Hz and strain $\gamma = 0.01$ was applied for $t = 15$ min where as a result, the storage modulus $G'$ increases from around 72 Pa to around 114 Pa. In shear start up test, both the stress overshoot and the corresponding strain increase with the shear rate $\dot{\gamma}$ (0.05 s$^{-1}$ to 0.5 s$^{-1}$). Inset shows the stress overshoot values versus shear rate
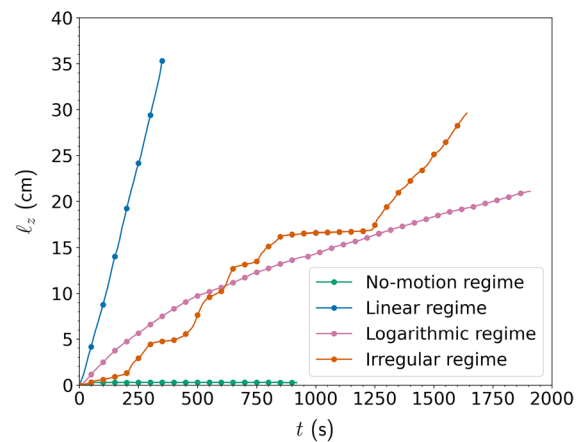


**Fig. 5** Sphere behavior along its path $\ell_z$ in TEMPO-CNF 0.58 wt%. Quantitatively different regimes of motion are observed for different sphere diameters $d_s$ and aging time $t_a$ of the sample. They are further classified to four categories

in Fig. 5. These regimes, which are observable depending on the diameter of the sphere $d_s$ and the aging time $t_a$ of the sample, are the following:

1.  No-motion regime: the sphere remains jammed at its initial position for extended periods of time;

2. Linear regime: the sphere falls rapidly through the sample with a specific velocity;
3. Logarithmic regime: the sphere velocity progressively decreases and never reaches a steady value within the observation window;
4. Irregular regime: the sphere moves irregularly in a sequence of alternating linear and no-motion regimes.

We classify trajectories according to a criterion similar to Sgreva et al. (2020). For each regime, the total displacement of the sphere can be characterized as follows: In the no-motion regime, the stress field imposed by the weight of the sphere is not sufficient to break down the cellulose fibers structure. As a result, the sphere either fails to move or moves less than 5 cm after a long time. In the logarithmic regime, the sphere may end stationary in the middle of the container or reach the container bottom. On the contrary in linear and irregular regimes, the sphere always travels through the entire material.

We first notice that there is a halting time $\Delta t$ in which the sphere is required to overcome the yield stress associated with the local fibril network. When this halting time tends to zero, the sphere does not stop at any intermediate point. This behavior is associated with either a linear or logarithmic regime (Fig. 5). We next study these two regimes, so that the motion is described with a linear or semi-logarithmic fit. The goodness of the fit is determined by the root-mean-square error (RMSE) and both values, $\text{RMSE}_{lin}$ and $\text{RMSE}_{log}$, are compared to determine the regime (Fig. 6a). The results illustrate the validity of the linear and logarithmic regimes. The ratio $\text{RMSE}_{lin}/\text{RMSE}_{log}$ determines the logarithmic regime: if the ratio is larger than unity the sedimentation is better represented by a logarithmic fit.

Finally, the intermittent regime is defined when the sphere locally halts for some time of $\Delta t$ s to overcome the yield stress. For this stop-and-go behavior, the sphere trajectory is irregular (Fig. 5), possibly mixed with a linear or logarithmic regime. Then to differentiate it from other regimes, we fit a linear curve and evaluate the goodness of the fit. To do this, we compute the mean velocity $\bar{v}_z$ of data and its standard deviation $\text{std}(v_z)$. Then, the linear regime is defined by two conditions: $\text{RMSE}_{lin} < \text{RMSE}_{log}$ and $\text{std}(v_z)/\bar{v}_z < \mathcal{T}$ for some threshold $\mathcal{T}$. Based on the measurement error, we estimate the threshold
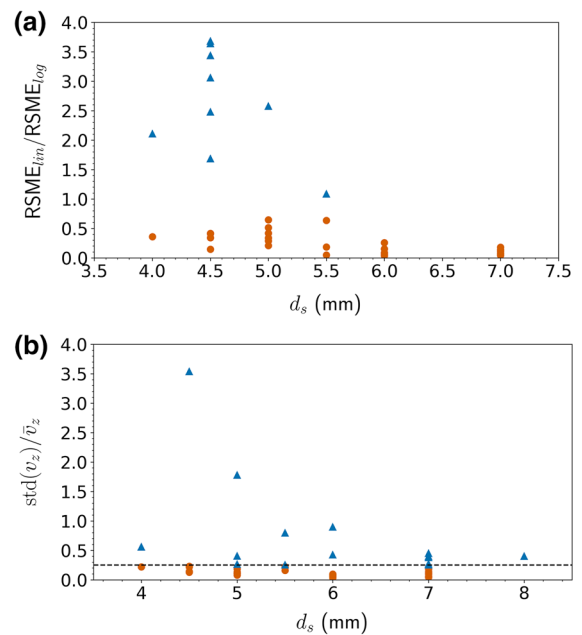


**Fig. 6** **a** Comparison of root-mean-square error (RMSE) for linear $\text{RMSE}_{lin}$ and logarithmic regimes $\text{RMSE}_{log}$. Red circles indicate a better linear fit whereas blue triangles a better semilog fit. **b** Ratio $\text{std}(v_z)/\bar{v}_z$ for those falling profiles that have been linearly fitted. The threshold $\mathcal{T}$ (black dashed line) is set to 0.25, below (above) which linear (irregular) regime is found, respectively. Linear regime: red circles; irregular regime: blue triangles

$\mathcal{T} = 0.25$, below which all linear cases are located as Fig. 6b shows. Thresholding reveals in a total of 15 experiments that exhibit irregular motion (the blue triangles in Fig. 6b) independent of the sphere diameters $d_s$.

Structural model

The wide variety of regimes is a consequence of the material internal structure, where above a specific concentration, the fluid behavior changes (Bonn et al. 2017). Coussot et al. (2002) proposed a simple $\lambda$-model, in which the time evolution of the structural parameter is governed by the aging (restructuring) and shear rejuvenation (destructuring) terms:

$$\frac{d\lambda}{dt} = \frac{1}{\theta} - \alpha\lambda\dot{\gamma} \tag{2}$$

Here, $\lambda$ assumed to increase with a constant rate of $1/\theta$, where $\theta$ is the characteristic restructuring time scale. Destructuring time scale considered

proportional to both the shear rate $\dot{\gamma}$ and the state degree of the structure $\lambda$, in which $\alpha$ is a material-dependent parameter. The competition between these two terms controls the settling behavior, and therefore, the characteristic of each settling regime.

This model suffices to discuss many of the features we observe in experiments. In rheology measurements, the hysteresis loop is governed by the ratio between the restructuring and destructuring rates (Iotti et al. 2011). When the destructuring rate, proportional to the rate of shear, tends to zero, the material becomes aged and displays more elastic solid features (Fig. 3). In Stokes' experiments, the model adequately explains different settling behaviors, as we will explain later on. On the contrary, the $\lambda$-model involves a single time scale insufficient to explain the full complexity present in TEMPO-CNFs (Koponen 2020). Thus, describing the material quantitatively requires a more precise and detailed model to be developed (Puisto et al. 2012; Mohtaschemi et al. 2014; Mwasame et al. 2019).

### No-motion regime

In this regime, since the weight of the sphere is not enough to overcome the yield stress $\sigma_T$, the internal structure remains unbroken ($1/\theta \gg \alpha\lambda\dot{\gamma}$). Therefore, we can estimate the yield stress based on the normal force generated by the sphere as $\sigma_T = gd_s^{min}\Delta\rho/21$, being $\Delta\rho = \rho_s - \rho_f$ (as we show in the following section, Eq. 4). Table 2 shows the threshold stress imposed on the fluid by the smallest sphere of diameter $d_s$ that is incapable of penetrating the fluid at all. This value certainly grows as the aging time increases.

### Linear regime

The linear regime is the classic behavior that a sphere adopts in a Newtonian fluid, and it was also reported

in simple and thixotropic yield stress fluids (Ferroir et al. 2004; Tabuteau et al. 2007; Fazilati et al. 2017). The regime can be described using two dimensionless numbers: the Bingham $Bi = \sigma_T/(K(v/d_s)^n)$ and yield $Y = 3\sigma_T/(gd_s\Delta\rho)$. Earlier studies for Carbopol gel (Tabuteau et al. 2007) and aqueous dispersions of superabsorbent polymers (Sgreva et al. 2020) have shown that the relationship between those numbers is given by:

$$\frac{1}{Y} = 7 + \frac{8.52}{Bi} \tag{3}$$

This equation may be rewritten into a Herschel-Bulkley type of relation (see Eq. 1):

$$\frac{gd_s\Delta\rho}{3} = 7\sigma_T + 8.52K\left(\frac{v_z}{d_s}\right)^n \tag{4}$$

We then proceed to determine the traveling velocity $v_z$ of the sphere. Figure 7 shows the experimental data (dots) together with the linear relation of Eq. 4 (solid lines), which is still valid for TEMPO-CNFs. Interestingly, for the unaged case, we find that the exponent is $n = 0.35$, as we showed for the flow curve (see Fig. 2b). Similarly, the effective yield stress and consistency are $\sigma_T = 10.15$ Pa and $K = 9.64$ Pa $\cdot$ s$^n$, respectively, which are comparable with values obtained in the rheology measurement.
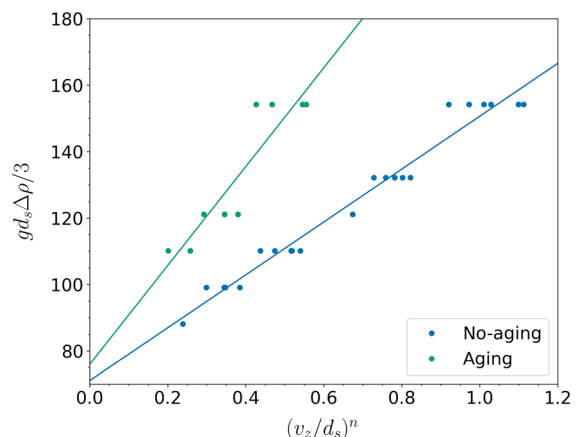


**Fig. 7** Stress induced by the sphere to the fluid as a function of the $(v_z/d_s)^n$. The data is fitted with a Herschel-Bulkley model (Sgreva et al. 2020), with exponent $n = 0.35$ and $n = 0.44$ for the material with no-aging and aging history, respectively. 'Aging' case includes all experiments with initial aging time larger than zero, resulting in linear sphere motion

**Table 2** Smallest sphere of diameter $d_s^{min}$ that does not penetrate the material with the aging time $t_a$

| $t_a$ (s) | $d_s^{min}$ (mm) | $\sigma_T$ (Pa) |
|---|---|---|
| 0 | 3.5 | 11 |
| 1800 | 4 | 12.6 |
| 432000 | 5 | 15.7 |

According to Eq. 2, when the aging time increases, the internal structure of the sample is reinforced, and thus a higher equivalent induced shear rate ($v_z/d_s$) is required. Therefore, the exponent increases to $n = 0.44$ as can be seen in Fig. 7. In addition, the effective yield stress and consistency increase to $\sigma_T = 10.85$ Pa and $K = 18.02$ Pa $\cdot$ s$^n$, respectively.

Irregular regime

Figure 8 displays the settling velocity of four typical irregular cases. In some short aged gels, traveling time into the material can be longer than the aging time, such as for $d_s = 5$ mm at $t_a = 221$ min. Thus away from the sphere, the restructuring of the cellulose fibers continuously occurs during the experiment. This leads to a situation where the sphere enters a different material state than at the beginning of the experiment. Oftentimes for several days aged samples, chaotic stop-go cycles can be witnessed such as for $d_s = 5.5$ mm at $t_a = 5$ d or $d_s = 7$ mm at $t_a = 16$ mm. It implies that the stress field around the sphere is affected by the local configuration of the fiber network even though the gravitational-induced stress remains constant. As a result, the sphere-gel interaction suggests a local halting time $\Delta t$, depending on the size of the sphere $d_s$ and the aging time $t_a$.

The irregular settling for appropriately short $\Delta t$ can be addressed as a semi-oscillatory motion such as in a case of $d_s = 7$ mm at $t_a = 300$ min.

Previously it has been shown that the irregular motion in a polymer gel is a consequence of the size of the sphere being comparable with the size distribution of grain particles of the gel where the non-homogeneity of the gel arises and influences the sphere-gel interaction Sgreva et al. (2020). We expect a similar phenomenon drives the occurrence of the irregular regime in TEMPO-CNFs. The difference, however, is that here the sphere deals with fibril flocs (Koponen 2020; Saarinen et al. 2014) the size and configuration of which evolves due to aging and rejuvenating processes that do not develop at the same rates in the whole sample, judging from fig. 8. This leads to different yield stress, viscosity, and elastic modulus at each moment in front of the sphere, which changes the halting time $\Delta t$ of penetrating the sphere.

Irregular regime can be obtained from the equation of motion of the settling sphere (Arigo and McKinley 1997; Von Kann et al. 2013), which is described by:

$$m\ddot{z} - m^*g = D(z, \dot{z}, t) \qquad (5)$$

where $m^*$ is the sphere's mass with the buoyancy correction and $D$ is the drag force. To solve this equation,



**Fig. 8** Settling velocity in vertical direction (z-axis) for four typical cases of irregular regime
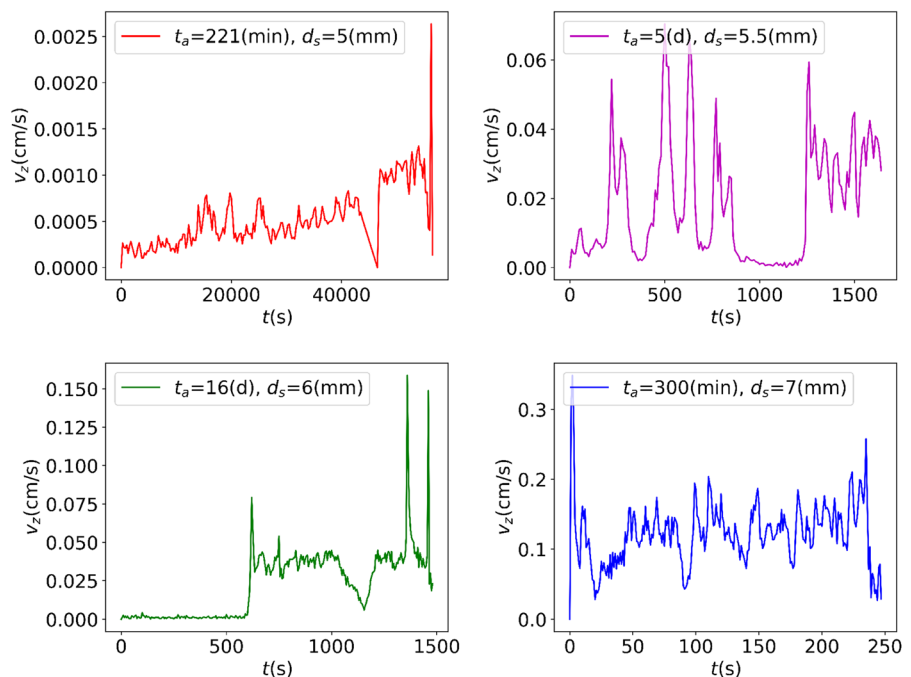
the functional shape of the stress considering both viscoelastic and thixotropic components and the yield stress is required. In general term, the stress is given by $\sigma = \sigma(\eta, \dot{\gamma}, t, \dot{\sigma})$ that for instance, considering the Maxwell viscoelastic model, it can read (Lehtinen et al. 2013; Armstrong et al. 2016):

$$\sigma = \eta(\lambda)\dot{\gamma} - \frac{\eta(\lambda)}{G_0(\lambda)}\frac{\partial \sigma}{\partial t} \tag{6}$$

where $G_0(\lambda)$ is the shear modulus. Then, depending on the drag force on the surface of the sphere, $D$, a function of $\sigma(\eta, \dot{\gamma}, t, \dot{\sigma})$, the velocity of the sphere, $\dot{z}$, follows:

$$-\dot{z} = \frac{\dot{D}}{G^*} + \frac{D}{\eta^*} \tag{7}$$

A particular solution to the set of equations was shown by Von Kann et al. (2013), where the frequency of oscillation depends on $\eta$ and $G_0$. For a thixotropic gel, however, $G^*$ and $\eta^*$ couple to the micro-structure and a solution of the structural constitutive model (Eq. 2) in time and space are involved. Utilizing the rheological tests, we have shown that for TEMPO-CNFs, $G^*$ and $\eta^*$, are shear history-dependent, which results in the occurrence of multiple frequencies of oscillation and manifests itself by a complete irregular motion (see Fig. 5). However, future numerical simulations will help to more thoroughly formulate this complex settling.

In addition, to better understand this regime, we compute the drag correction factor of time-dependent elasto-viscous fluids (Mrokowska and Krztoń-Maziopa 2019):

$$K_D = \frac{v_s}{v_z} \tag{8}$$

where $v_z$ and $v_s$ are respectively denoting average traveling velocity of the sphere in TEMPO-CNFs and the terminal settling velocity in an equivalent Stokes' flow:

$$v_s = \frac{g(\rho_s - \rho_f)d_s^2}{18\eta_0} \tag{9}$$

where based on the the flow curve data at $\dot{\gamma} = 1000 \text{ s}^{-1}$, the viscosity $\eta_0 = 0.17 \text{ Pa} \cdot \text{s}$.

Moreover, the Deborah number $De = \tau/\tau_z$ is defined as the ratio of the fluid elastic relaxation

time, $\tau$, to the average traveling time $\tau_z$ of the sphere into the fluid. According to the SAOS experimental data, the elastic relaxation time follows a logarithmic growth with aging time (Shaukat et al. 2009):

$$\tau = \frac{G'}{2\pi f G''} = \tau_0 + a \log(t_a) \tag{10}$$

where $\tau_0 = 0.493$ s and $a = 0.124$. Figure 9 indicates a decreasing trend for $K_D$ with De, similar to other viscoelastic fluids. Moreover, the data implies that settling in TEMPO-CNFs is particularly slower than in a simple Stokes fluid.

## Conclusion

The time-dependent flow behavior of TEMPO nanofibrillated cellulose gels (0.58 wt%) was investigated utilizing two different methods: a rheological characterization and settling of a solid spherical object.

A hysteresis loop was observed by sweeping down and up the shear rate in the flow curve measurement, which increased with point time $\delta t$. Consequently, the flow behavior for the present material batch was indeed dependent on the shear history. When the hysteresis is relatively small, the Herschel-Bulkley model with an exponent $n = 0.358$ could be applied to adequately capture the flow curve. The model could also imply that the yield stress slightly decreases with
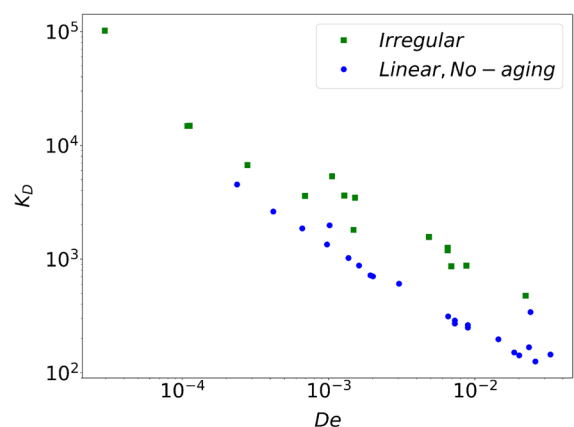
**Fig. 9** Drag correction factor $K_D$ as a function of the Deborah number De. Green square stands for the irregular regime and blue circle indicates data for the linear regime in rejuvenated (no-aging) samples

increasing $\delta t$. However, it cannot explain the hysteresis in the flow curve. Additionally, monitoring the structure build-up by applying the SAOS experiment revealed that the storage modulus $G'$ follows a logarithmic behavior with time, where a longer waiting time in the SAOS test resulted in more development of a stress overshoot in the subsequent shear start-up test. Increasing the imposed shear rate in the shear start-up measurement also indicated an increase in the stress overshoot, which relaxed at higher strain values towards the values measured in the flow curve experiment. In conclusion, the rheological data suggested age-dependent moduli, and this manifests in age-dependent yield properties, which can be observed *e.g.* as the stress overshoot during the shear start-up experiment.

In line with other simple and thixotropic yield stress fluids (Ferroir et al. 2004; Fazilati et al. 2017; Sgreva et al. 2020), the settling motion of the sphere exhibited a variety of regimes as seen in Fig. 10.

The existence of these regimes can be justified as follows. Judging by Figure 7 and Table 2, a specific threshold yield stress value is associated with each aging time. Small spheres cannot overcome this stress leading to the no-motion regime. In contrast, large spheres which impose a stress above the threshold value fall with a constant velocity leading to the linear settling regime. Between these two sizes, two separate regimes appear, the logarithmic and an irregular
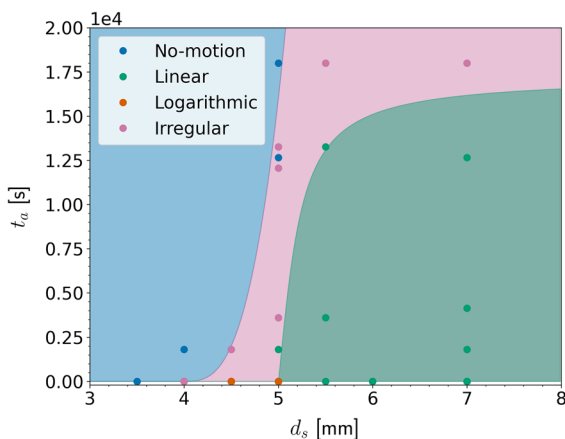
one. The logarithmic regime is mostly apparent in rejuvenated samples (no-aging). The irregular regime highlights our proposition that aging is also a local phenomenon, and the same material will have regions of different yield stresses despite the same shear history.

From a modeling perspective, a linear relationship between the effective settling velocity and the weight of the sphere can be defined for the linear regime where the sphere descends without significant perturbations. Thus, a Herschel-Bulkley type model was fitted to the settling data in this regime where the exponent and the yield stress perfectly conform to the rheological measurements, $n = 0.35$ and $\sigma_T = 10.15$ Pa (rejuvenated samples). For aged samples, the exponent $n$ and the yield stress increase to $n = 0.44$ and $\sigma_T = 10.85$ Pa.

In the irregular regime, as the transit time of the sphere decreases, the CNF response time is important (Eq. 2), and for longer aging time, the sphere velocity data displayed a scatter around the linear motion. Therefore, a mean velocity based on the data was computed. The drag correction factor $K_D$ for this material, calculated from the mean velocity, decreases as the Deborah number De increases. In the irregular and logarithmic regimes, our model comparisons would need to be extended to a more realistic geometry involving a joint simulation of the material (aging) response and the sphere settling dynamics.

Contrary to other low-density gels and Laponite in particular, our TEMPO-CNF samples required a longer aging time to recreate the structure and even rejuvenated samples seemed to possess a considerable yield stress. With aging, the yield stress increased as anticipated for a thixotropic-viscoelastic yield stress gel. Under specific conditions involving an appropriate mass for the solid sphere, an irregular settling can be observed. Moreover, depending on the local halting time $\Delta t$ stoppage periods appear in the irregular regime which this feature distinguishes it from a semi-oscillatory settling in Laponite B® (1.5 wt%) (Fazilati et al. 2017), for instance. Long traveling time in certain irregular cases indicates that the restructuring time scale is more dominant in the present system compared to for instance Laponite XLG® (2.8 wt%) (Biswas et al. 2021). These dissimilarities most likely relate to the completely different internal particle structures between the present system and the ones studied before.



**Fig. 10** Regions for the four different behaviors of the settling sphere. The plot displays zones as a function of the sphere diameter $d_s$ (x-axis) and the aging time $t_a$ (y-axis). The transitions between different regions are not exact and should be viewed as qualitative rather than quantitative

**Declarations**

**Conflict of interest** The authors declare that they have no conflict of interest.

# References

Arigo MT, McKinley GH (1997) The effects of viscoelasticity on the transient motion of a sphere in a shear-thinning fluid. J Rheol 41(1):103–128. https://doi.org/10.1122/1.550803

Arigo MT, McKinley GH (1998) An experimental investigation of negative wakes behind spheres settling in a shear-thinning viscoelastic fluid. Rheol Acta 37(4):307–327. https://doi.org/10.1007/s003970050118

Armstrong MJ, Beris AN, Rogers SA (2016) Dynamic shear rheology of a thixotropic suspension: comparison of an improved structure-based model with large amplitude oscillatory shear experiments. J Rheol 60:433–450. https://doi.org/10.1122/1.4943986

Barnes HA (1997) Thixotropy - a review. J Nonnewton Fluid Mech 70(1):1–33. https://doi.org/10.1016/S0377-0257(97)00004-9

Benzi R, Divoux T, Barentin C, Manneville S, Sbragaglia M, Toschi F (2021) Stress overshoots in simple yield stress fluids. Phys Rev Lett 127(14):148003. https://doi.org/10.1103/PhysRevLett.127.148003

Biswas R, Saha D, Bandyopadhyay R (2021) Quantifying the destructuring of a thixotropic colloidal suspension using falling ball viscometry. Phys Fluids 33(1):013103. https://doi.org/10.1063/5.0035093

Bonn D, Denn MM, Berthier L, Divoux T, Manneville S (2017) Yield stress materials in soft condensed matter. Rev Mod Phys 89:035005. https://doi.org/10.1103/RevModPhys.89.035005

Coussot P, Nguyen QD, Huynh HT, Bonn D (2002) Avalanche behavior in yield stress fluids. Phys Rev Lett 88:175501. https://doi.org/10.1103/PhysRevLett.88.175501

Dimic-Misic K, Puisto A, Gane P, Nieminen K, Alava M, Paltakari J, Maloney T (2013) The role of MFC/NFC swelling in the rheological behavior and dewatering of high consistency furnishes. Cellulose 20(6):2847–2861. https://doi.org/10.1007/s10570-013-0076-3

Divoux T, Barentin C, Manneville S (2011) Stress overshoot in a simple yield stress fluid: an extensive study combining rheology and velocimetry. Soft Matter 7(19):9335–9349. https://doi.org/10.1039/C1SM05740E

Divoux T, Grenard V, Manneville S (2013) Rheological hysteresis in soft glassy materials. Phys Rev Lett 110(1):018304. https://doi.org/10.1103/PhysRevLett.110.018304

Dollet B, Graner F (2007) Two-dimensional flow of foam around a circular obstacle: local measurements of elasticity, plasticity and flow. J Fluid Mech 585:181–211. https://doi.org/10.1017/S0022112007006830

Fazilati M, Maleki-Jirsaraei N, Rouhani S, Bonn D (2017) Quasi-periodic and irregular motion of a solid sphere falling through a thixotropic yield-stress fluid. Appl Phys Express 10(11):117301. https://doi.org/10.7567/APEX.10.117301

Ferroir T, Huynh H, Chateau X, Coussot P (2004) Motion of a solid object through a pasty (thixotropic) fluid. Phys Fluids 16(3):594–601. https://doi.org/10.1063/1.1640372

Fneich F, Ville J, Seantier B, Aubry T (2019) Structure and rheology of aqueous suspensions and hydrogels of cellulose nanofibrils: Effect of volume fraction and ionic strength. Carbohydr Polym 211:315–321. https://doi.org/10.1016/j.carbpol.2019.01.099

Gueslin B, Talini L, Herzhaft B, Peysson Y, Allain C (2006) Flow induced by a sphere settling in an aging yield-stress fluid. Phys Fluids 18(10):103101. https://doi.org/10.1063/1.2358090

Gueslin B, Talini L, Peysson Y (2009) Sphere settling in an aging yield stress fluid: link between the induced flows and the rheological behavior. Rheol Acta 48(9):961–970. https://doi.org/10.1007/s00397-009-0376-6

Hubbe MA, Tayeb P, Joyce M, Tyagi P, Kehoe M, Dimic-Misic K, Pal L (2017) Rheology of nanocellulose-rich aqueous suspensions: a review. BioResources 12(4):9556–9661

Iotti M, Gregersen OW, Moe S, Lenes M (2011) Rheological studies of microfibrillar cellulose water dispersions. J Polym Environ 19:137–145. https://doi.org/10.1007/s10924-010-0248-2

Koponen AI (2020) The effect of consistency on the shear rheology of aqueous suspensions of cellulose micro-and nanofibrils: a review. Cellulose 27: 1879--1897, https://doi.org/10.1007/s10570-19-02908-w

Isogai A, Saito T, Fukuzumi H (2011) TEMPO-oxidized cellulose nanofibers. Nanoscale 3(1):71–85. https://doi.org/10.1039/C0NR00583E

Lasseuguette E, Roux D, Nishiyama Y (2008) Rheological properties of microfibrillar suspension of TEMPO-oxidized pulp. Cellulose 15(3):425–433. https://doi.org/10.1007/s10570-007-9184-2

Lehtinen A, Puisto A, Illa X, Mohtaschemi M, Alava MJ (2013) Transient shear banding in viscoelastic Maxwell fluids. Soft Matter 9:8041–8049. https://doi.org/10.1039/C3SM50988E

Leppiniemi J, Lahtinen P, Paajanen A, Mahlberg R, Metsä-Kortelainen S, Pinomaa T, Pajari H, Vikholm-Lundin I, Pursula P, Hytönen VP (2017) 3D-printable bioactivated nanocellulose-alginate hydrogels. ACS Appl Mater Interfaces 9(26):21959–21970. https://doi.org/10.1021/acsami.7b02756

Levanic J, Šenk V, Nadrah P, Poljanšek I, Oven P, Haapala A (2020) Analyzing tempo-oxidized cellulose fiber morphology: new insights into optimization of the oxidation process and nanocellulose dispersion quality. ACS Sustain Chem Eng 8(48):17752–17762. https://doi.org/10.1021/acssuschemeng.0c05989

Li MC, Wu Q, Moon RJ, Hubbe MA, Bortner MJ (2021) Rheological aspects of cellulose nanomaterials: governing factors and emerging applications. Adv Mater 33(21):2006052. https://doi.org/10.1002/adma.202006052

Liao J (2021) Rheological characterization of cellulose nanomaterials for quality control and processing. PhD thesis, Georgia Institute of Technology

Liao J, Pham KA, Breedveld V (2021) Tempo-CNF suspensions in the viscoelastic regime: capturing the effect of morphology and surface charge with a rheological parameter. Cellulose 28(2):813–827. https://doi.org/10.1007/s10570-020-03572-1

Martoïa F, Perge C, Dumont PJ, Orgéas L, Fardin MA, Manneville S, Belgacem MN (2015) Heterogeneous flow kinematics of cellulose nanofibril suspensions under shear. Soft Matter 11(24):4742–55. https://doi.org/10.1039/C5SM00530B

Mohtaschemi M, Puisto A, Illa X, Alava MJ (2014) Rheology dynamics of aggregating colloidal suspensions. Soft Matter 10(17):2971–2981. https://doi.org/10.1039/C3SM53082E

Moseley K, Fairweather M, Harbottle D (2019) Settling dynamics of two identical vertically aligned spheres in a thixotropic fluid. J Nonnewton Fluid Mech 271:104146. https://doi.org/10.1016/j.jnnfm.2019.104146

Mrokowska MM, Krztoń-Maziopa A (2019) Viscoelastic and shear-thinning effects of aqueous exopolymer solution on disk and sphere settling. Sci Rep 9(1):1–13. https://doi.org/10.1038/s41598-019-44233-z

Mwasame PM, Beris AN, Diemer RB, Wagner NJ (2017) A constitutive equation for thixotropic suspensions with yield stress by coarse-graining a population balance model. AIChE J 63(2):517–531. https://doi.org/10.1002/aic.15574

Nechyporchuk O, Belgacem MN, Pignon F (2014) Rheological properties of micro-/nanofibrillated cellulose suspensions: wall-slip and shear banding phenomena. Carbohydr

Polym 112:432–439. https://doi.org/10.1016/j.carbpol.2014.05.092

Nechyporchuk O, Belgacem MN, Pignon F (2016) Current progress in rheology of cellulose nanofibril suspensions. Biomacromolecules 17(7):2311–2320. https://doi.org/10.1021/acs.biomac.6b00668

Pääkkönen T, Dimic-Misic K, Orelma H, Pönni R, Vuorinen T, Maloney T (2016) Effect of xylan in hardwood pulp on the reaction rate of tempo-mediated oxidation and the rheology of the final nanofibrillated cellulose gel. Cellulose 23(1):277–293. https://doi.org/10.1007/s10570-015-0824-7

Pöhler T, Ketoja JA, Lappalainen T, Luukkainen VM, Nurminen I, Lahtinen P, Torvinen K (2020) On the strength improvement of lightweight fibre networks by polymers, fibrils and fines. Cellulose 27:6961–6976. https://doi.org/10.1007/s10570-020-03263-x

Puisto A, Illa X, Mohtaschemi M, Alava MJ (2012) Modeling the rheology of nanocellulose suspensions. NPPRJ 27:277–281. https://doi.org/10.3183/npprj-2012-27-02-p277-281

Poling-Skutvik R, McEvoy E, Shenoy V, Osuji CO (2020) Yielding and bifurcated aging in nanofibrillar networks. Phys Rev Mater 4:102601. https://doi.org/10.1103/PhysRevMaterials.4.102601

Putz A, Burghelea T, Frigaard I, Martinez D (2008) Settling of an isolated spherical particle in a yield stress shear thinning fluid. Phys Fluids 20(3):033102. https://doi.org/10.1063/1.2883937

Radhakrishnan R, Divoux T, Manneville S, Fielding SM (2017) Understanding rheological hysteresis in soft glassy materials. Soft Matter 13(9):1834–1852. https://doi.org/10.1039/C6SM02581A

Saarinen T, Haavisto S, Sorvari A, Salmela J, Seppälä J, (2014) The effect of wall depletion on the rheology of microfibrillated cellulose water suspensions by optical coherence tomography. Cellulose 21:1261. https://doi.org/10.1007/s10570-014-0187-5

Sanandiya ND, Vasudevan J, Das R, Lim CT, Fernandez JG (2019) Stimuli-responsive injectable cellulose thixogel for cell encapsulation. Int J Biol Macromol 130:1009–1017. https://doi.org/10.1016/j.ijbiomac.2019.02.135

Šebenik U, Krajnc M, Alič B, Lapasin R (2019) Ageing of aqueous TEMPO-oxidized nanofibrillated cellulose dispersions: a rheological study. Cellulose 26(2):917–931. https://doi.org/10.1007/s10570-018-2128-1

Šebenik U, Lapasin R, Krajnc M (2020) Rheology of aqueous dispersions of laponite and tempo-oxidized nanofibrillated cellulose. Carbohydr Polym 240:116330. https://doi.org/10.1016/j.carbpol.2020.116330

Sgreva NR, Davaille A, Kumagai I, Kurita K (2020) Interaction between a falling sphere and the structure of a non-newtonian yield-stress fluid. J Nonnewton Fluid Mech 284:104355. https://doi.org/10.1016/j.jnnfm.2020.104355

Shaukat A, Joshi YM, Sharma A (2009) Tensile deformation and failure of thin films of aging Laponite suspension. Ind Eng Chem Res 48(17):8211–8218. https://doi.org/10.1021/ie9006326

Skogberg A, Mäki AJ, Mettänen M, Lahtinen P, Kallio P (2017) Cellulose nanofiber alignment using

evaporation-induced droplet-casting, and cell alignment on aligned nanocellulose surfaces. Biomacromolecules 18(12):3936–3953. https://doi.org/10.1021/acs.biomac.7b00963

Tabuteau H, Coussot P, de Bruyn JR (2007) Drag force on a sphere in steady motion through a yield-stress fluid. J Rheol 51(1):125–137. https://doi.org/10.1122/1.2401614

Viitanen L, Koivisto J, Puisto A, Alava M, Santucci S (2019) Probing the local response of a two-dimensional liquid foam. Eur Phys J B 92(2):1–6. https://doi.org/10.1140/epjb/e2019-90402-x

Von Kann S, Snoeijer JH, Lohse D, van der Meer D (2011) Nonmonotonic settling of a sphere in a cornstarch suspension. Phys Rev E 84:060401. https://doi.org/10.1103/PhysRevE.84.060401

Von Kann S, Snoeijer JH, van der Meer D (2013) Velocity oscillations and stop-go cycles: the trajectory of an object settling in a cornstarch suspension. Phys Rev E 87:042301. https://doi.org/10.1103/PhysRevE.87.042301